$^{13}C \rightarrow {}^1H$ transfer of light-induced hyperpolarization allows for selective detection of protons in frozen photosynthetic reaction center

Pavlo Bielytskyi [a], Daniel Gräsing [a], Kaustubh R. Mote [b], Karthick Babu Sai Sankar Gupta [c], Shimon Vega [d], P.K. Madhu [b,e], A. Alia [c,f], Jörg Matysik [a,*]

[a] *Institut für Analytische Chemie, Universität Leipzig, Linnéstraße 3, D-04103 Leipzig, Germany*
[b] *TIFR Centre for Interdisciplinary Sciences, Tata Institute of Fundamental Research, 36/P Gopanpally Village, Serilingampally Mandal, Ranga Reddy District, Hyderabad 500107, India*
[c] *Leiden Institute of Chemistry, Leiden University, Einsteinweg 55, 2301 RA Leiden, The Netherlands*
[d] *Department of Chemical Physics, Weizmann Institute of Science, 76100 Rechovot, Israel*
[e] *Department of Chemical Sciences, Tata Institute of Fundamental Research, Homi Bhabha Road, Colaba, Mumbai 400005, India*
[f] *Institut für Medizinische Physik und Biophysik, Universität Leipzig, Härtelstr. 16-18, D-04107 Leipzig, Germany*

A R T I C L E   I N F O

A B S T R A C T

In the present study, we exploit the light-induced hyperpolarization occurring on ^{13}C nuclei due to the solid-state photochemically induced dynamic nuclear polarization (photo-CIDNP) effect to boost the NMR signal intensity of selected protons via inverse cross-polarization. Such hyperpolarization transfer is implemented into ^1H-detected two-dimensional ^{13}C–^1H correlation magic-angle-spinning (MAS) NMR experiment to study protons in frozen photosynthetic reaction centers (RCs). As a first trial, the performance of such an experiment is tested on selectively ^{13}C labeled RCs from the purple bacteria of *Rhodobacter sphaeroides*. We observed response from the protons belonging to the photochemically active cofactors in their native protein environment. Such an approach is a potential heteronuclear spin-torch experiment which could be complementary to the classical heteronuclear correlation (HETCOR) experiments for mapping proton chemical shifts of photosynthetic cofactors and to understand the role of the proton pool around the electron donors in the electron transfer process occurring during photosynthesis.

1. Introduction

NMR spectroscopy is one of the most versatile techniques to study the structure and dynamics of both organic and inorganic molecules. However, the main drawback of NMR spectroscopy as an analytical tool lies in its low sensitivity due to unfavorable nuclear Boltzmann polarization at thermal equilibrium and lack of selectivity especially for protons in the solid state. These issues become more apparent when characterizing large biomolecular systems such as membrane proteins, where low sensitivity and low resolution combine to be a great experimental challenge [1]. A range of different methods to increase the NMR sensitivity has been developed over the years in which a non-Boltzmann spin order is induced by physical or chemical means [2]. These methods, often summarized as "nuclear spin-hyperpolarization methods", despite being extremely effective in a wide range of applications, possess their own weaknesses, whether it is long-lasting hyperpolarization build-up, short lifetime of the produced hyperpolarization, occurrence of hyperpolarization only on specific type of nuclei or its high localization with inability to be used beyond a particular system. In order to take the most advantage of the hyperpolarization method in the context of a particular experiment, hyperpolarization transfers between different nuclei/molecules can be implemented. For example, the transfer of hyperpolarization, produced in a dissolution dynamic nuclear polarization (DNP) setup, from ^1H nuclei to ^{13}C [3,4] and to ^{15}N [5] allows for much higher polarization factors and greatly reduced experimental time as compared with direct DNP. Hyperpolarization produced on ^{129}Xe nuclei by spin-exchange optical pumping (SEOP) can be used to enhance the polarization of surface ^1H nuclei [6]. Polarization of ^{15}N spins can be achieved by INEPT-based transfer from ^1H nuclei in parahydrogen-induced polarization (PHIP) [7] and signal amplification by reversible exchange (SABRE) techniques [8]. Transfer of hyperpolarization produced by photochemically induced dynamic nuclear polarization (photo-CIDNP) in liquid phase from ^{15}N to ^1H allows to overcome a problem of poor spectral resolution of conventional liquid-state ^1H photo-CIDNP

* Corresponding author.
  E-mail address: joerg.matysik@uni-leipzig.de (J. Matysik).

experiments, thus opening a new means for studying protein folding [9].

Photo-CIDNP magic-angle-spinning (MAS) NMR, relying on the solid-state photo-CIDNP effect, is one of the members of the family of nuclear spin-hyperpolarization methods. Since its discovery in 1994 by Zysmilich and McDermott [10], it has been developed into an analytical tool for studying the electronic structures of small photosynthetic cofactors embedded in huge protein membrane complexes, since it provides high nuclear spin order that can be observed as strong signal enhancement (by a factor of 10,000–80,000 for ^{13}C) by MAS NMR experiments [11]. The effect occurs in all natural photosynthetic reaction centers (RCs) studied so far [12,13], and also in a blue-light photoreceptor, the phototropin mutant LOV1-C57S [14]. In these systems, the spin-correlated radical pair (SCRP) is formed between electron donor and acceptor after initial electron transfer upon light excitation. During the lifetime of SCRP, up to three different solid-state mechanisms operate in parallel for nuclear hyperpolarization build-up [15,16]. Recently, these mechanisms have been interpreted in terms of level crossings and level anti-crossings concept (LCs and LACs), thus providing more general description of the occurrence of the effect [17]. The ability to reveal the electronic structures of the cofactors forming the SCRP upon photosynthetic charge-separation allows solid-state photo-CIDNP MAS NMR to become a unique instrument to study complex photosynthetic machineries even in membranes and cells without further isolation [18–20]. The RC of the purple bacteria *Rhodobacter (R.) sphaeroides* (the structure presented in Fig. SI 1) is considered to be paradigmatic for an entire class of RCs [21]. Successful combination of signal enhancement from selectively hyperpolarized ^{13}C nuclei with homonuclear correlation experiments allowed for unambiguous signal assignment of electron donor and acceptor in this bacterial RC [22–24]. On that basis, the molecular electronic structures of the cofactors forming the primary SCRP in the electronic ground state, the charge separated state, as well as molecular triplet state have been obtained [25].

The solid-state photo-CIDNP effect can be used in spin-torch experiments, in which the strongly enhanced ^{13}C polarization is transferred to the neighboring ^{13}C nuclei in the protein vicinity around SCRP via natural spin diffusion. Photosynthetic RCs are well-defined systems with constant geometrical constraints and environment, therefore they are very suitable for studying polarization transfer processes. The spin-torch approach would allow exploring the protein pocket around the photosynthetic cofactors, thus going beyond the current application limits of photo-CIDNP MAS NMR. However, this approach relies on the presence of the selective ^{13}C isotope labels in the protein pocket [26], which is not always feasible. The use of ^1H as an alternative nucleus, on the other hand, eliminates this need. Furthermore, direct ^1H information of the nearby amino acids would be itself a perfect probe to study the protein environment, such as the protonation state and the role of the hydrogen-bonding network around the electron donor in both ground and charge-separated state. Until now, however, the effect has been observed solely for ^{15}N and ^{13}C nuclei, and ^1H photo-CIDNP MAS NMR experiments have failed, unlike the case of liquids where direct ^1H photo-CIDNP NMR is common. One of the possible explanations for this fact is the strong magnetic-field dependence of the solid-state photo-CIDNP effect that puts certain restrictions on the observation field windows for different nuclei [27]. For solids, direct ^1H photo-CIDNP has been predicted to occur at magnetic fields close to the Earth's magnetic field [17,28]. Presently, our shuttle MAS NMR setup [27] is suitable for the generation of solid-state photo-CIDNP in the stray field of the NMR magnet in the mT range, and we aim for an extension towards Earth's magnetic field. Furthermore, the fast spin diffusion via the network of strongly coupled protons is expected to dimin-

ish the locality of the generated ^1H photo-CIDNP similar to ^{13}C photo-CIDNP on uniformly ^{13}C-labelled RC [26]. Therefore, further development of the spin-torch approach was hampered. As the result, even such extensively studied system as RC from *R. sphaeroides* still lacks comprehensive information about the role of the protein pocket around the photosynthetic cofactors in tuning their properties, especially the state of protons under dark and light conditions. Previous studies of the photosynthetic RC from purple bacteria with electron paramagnetic resonance (EPR) techniques suggested the crucial role of the hydrogen-bonding networks around the electron donor in distributing the electron spin density on donor radical cation and controlling the oxidative potential [29,30]. Site-specific mutations resulting in adding or removing hydrogen bonds between the special pair dimer and surrounding amino acids showed the alteration of the oxidation potential of the electron donor [31]. The amino acid environment of the electron donor of plant photosystem II (PSII) was suggested to control the unique redox properties [32]. The complexity of the photosynthetic systems and the current limitation in the MAS spinning frequencies for sapphire rotors therefore make standard ^1H MAS NMR experiments very challenging. The heteronuclear spin-torch experiments in which the hyperpolarization created on ^{13}C or ^{15}N nuclei of the active cofactors is selectively transferred to the protons of close environment could be an elegant strategy to obtain more complete information about the functional principles of both the photosynthetic cofactors and their close protein environment. In solution state, heteronuclear polarization transfers based on J-couplings were successfully implemented in the context of heteronuclear correlation experiments (HETCORs) [9,33–35]. With advances in the field of ^1H detection in solid-state MAS NMR [36,37], the emergence of similar types of photo-CIDNP experiments is expected to be possible also in frozen photosynthetic proteins.

In the present study, we demonstrate the possibility to transfer hyperpolarization generated by the solid-state photo-CIDNP effect on ^{13}C nuclei to the nearby ^1H nuclei in the core of the frozen photosynthetic RC by inverse cross-polarization (CP). We propose two-dimensional ^{13}C–^1H correlation MAS NMR experiment to study the proton environment of the SCRP in photosynthetic RCs, thus broadening the range of applications of photo-CIDNP MAS NMR as an analytical tool.

2. Materials and methods

2.1. Sample preparation

The selective ^{13}C labeling of the BChl *a* and BPheo *a* cofactors in the reaction center of *R. sphaeroides WT* was achieved by feeding 5-^{13}C-δ-aminolevulinic acid (5-ALA), as described earlier [38]. The 5-ALA (99% ^{13}C enriched) was purchased from Cambridge Isotope Laboratories. Isolation of the RCs was carried out following established protocol [39]. The quinones were removed by incubating the RCs at a concentration of 0.6 µM in 4% LDAO, 10 mM *o*-phenanthroline, 10 mM Tris buffer, pH = 8.0, containing 0.025% LDAO and 1 mM EDTA [40].

2.2. NMR measurements

All NMR experiments were performed at 9.4 T with an AVANCE III NMR spectrometer equipped with a 4-mm double resonance MAS probe (Bruker, Karlsruhe, Germany). Approximately 5 mg of 5-ALA labeled RC complex embedded in LDAO micelles was loaded into a transparent 4-mm sapphire rotor and inserted into the MAS probe. The sample was frozen in the dark at slow spinning frequency of 400 Hz to ensure a homogeneous sample distribution

against the rotor walls [41]. After freezing, the stable sample temperature of 247 K was maintained by a temperature control unit. The spinning frequency of 8176 ± 10 Hz was regulated by a pneumatic control unit. The idle time of several hours prior to the NMR experiments was needed to equilibrate the temperature of the probe electronics in order to stabilize the ^{1}H wobble curve. The stable ^{1}H wobble curve is crucial as its unaccounted shift might lead to errors during the calibration of the ^{1}H chemical shift axis. Illumination of the sample was achieved by using the continuous illumination setup described previously [16]. It comprises a 1000-W xenon arc lamp with collimation optics, a water filter and glass filters, a focusing element and a light fiber bundle. The xenon arc lamp emits a sunlight-like spectrum covering a wide range of frequencies from the UV to the IR. The water filter cuts off the IR frequencies and prevents the disturbance of the spinning speed counter, working in the near-IR region. The UV part of the emission spectrum is removed by a set of glass filters. A fiber bundle is used to transfer the radiation from the collimation optics to the sample. A mechanical shutter is incorporated into the setup to assure a defined illumination time. Optimized ^{1}H and ^{13}C 90° pulse lengths were 2.5 and 3.0 μs, respectively. The ^{13}C NMR spectra were referenced to the COOH response of solid L-tyrosine hydrochloride at 172.1 ppm. Appropriately scaled ^{1}H dimension was referenced by assigning the midpoint of two methylene proton peaks of solid glycine to 3.52 ppm.

The data was processed with Bruker TopSpin 3.2 and plotted with MNova 12 (Mestrelab Research, S. L. Santiago de Compostela, Spain).

2.3. Windowed detection

Acquisition in analogue mode using windowed version of supercycled-phase-modulated Lee-Goldburg homonuclear decoupling (wPMLG3-S2) [42,43] was optimized by monitoring the splitting between the methylene protons of unlabeled glycine while keeping the MAS frequency at 8176 Hz and changing the following parameters: length of individual PMLG pulse, window duration, RF amplitude and the carrier offset [36,44]. In wPMLG3 decoupling, the basic unit consists of PMLG3 block (τ_{PMLG3}) and the acquisition window τ_w resulting in a cycle period of $\tau_c = \tau_{PMLG3} + \tau_w$. Each PMLG3 block consisted of 6 pulses with the following phases: 214.64°, 283.92°, 353.21°, 173.20°, 103.92° and 34.64° (m3p shape in TopSpin 3.2 library). A consecutive PMLG3 block is then repeated with 180° phase shift to complete S2 supercycle [42]. The optimal pulse length of each pulse in PMLG3 block was found to be 2.45 μs (τ_{PMLG3} = 14.70 μs), and the window duration τ_w was 4.95 μs. Therefore, the overall length of decoupling cycle time τ_c was equal to 19.65 μs, resulting in the characteristic frequency ν_c = 50.89 kHz. In order to avoid line broadening due to undesirable destructive PMLG interferences, it is required that $3\tau_c < \tau_r$ and $4\tau_c \neq \tau_r$ where τ_r is the rotor period [45,46]. In the present setup, the rotor period τ_r = 122.3 μs and τ_r/τ_c = 6.22, being far off of the obvious degeneracies. The RF amplitude during decoupling was set to 88372 Hz. The ^{1}H RF offset frequency was set to −2900 Hz during windowed acquisition to avoid RF-rotary-frequency lines and other artifacts falling over the spectral region of interest [47]. The scaling factor of 0.52 was determined on adamantane by plotting the dependence of the apparent offset shift against the actual offset change (Fig. SI 2) and was further used to correct the ^{1}H spectral width. Considering the possible difference of the RF nutation frequency in adamantane and the frozen protein, which might lead to slightly different scaling factor, the above procedure was repeated on the 5-ALA protein sample monitoring the shift of water peak. The same scaling factor was confirmed.

2.4. ^{13}C photo-CIDNP MAS NMR

The standard 1D ^{13}C photo-CINDP MAS NMR experiments were recorded with Hahn-echo sequence with 256 scans and 4 s relaxation delay. Swept-frequency two-pulse phase-modulation (SW$_f$-TPPM) heteronuclear decoupling [48] with 100 kHz RF field was used during the acquisition.

2.5. ^{13}C → ^{1}H hyperpolarization transfer and carbon acquisition

The 1D ^{13}C experiments were recorded with 256 scans and 4 s relaxation delay, resulting in 17 min measurement time each. The Lee-Goldburg CP (LGCP) [49] was optimized to satisfy both Hartmann-Hahn (HH) n = ±1 matching condition, with 61 kHz effective ^{1}H RF lock field and 70–100% ramp on ^{13}C channel. LGCP contact time was set to 80 μs, 500 μs and 4500 μs. SW$_f$-TPPM heteronuclear decoupling with 100 kHz RF field was used during the acquisition.

2.6. ^{13}C → ^{1}H hyperpolarization transfer and proton acquisition

The 1D windowed ^{1}H experiments were recorded with 2048 scans and 4 s relaxation delay, resulting in 2.5 h measurement time each. The LGCP was optimized to satisfy HH n = ±1 matching condition, with 61 kHz effective ^{1}H RF lock field and 70–100% ramp on ^{13}C channel. LGCP contact time was set to 80 μs, 500 μs and 4500 μs. The solvent suppression was achieved with repeating alternating X and Y pulses on-resonance with the water peak, with RF frequency of 20 kHz and total length of the saturation block of 100 ms. Exponential window function with line broadening of 50 Hz was applied prior to Fourier transformation. The spectra were phased according to U-^{13}C labelled L-alanine.

2.7. Photo-CIDNP ^{13}C → ^{1}H HETCOR MAS NMR experiments with proton acquisition

The 2D HETCOR spectra were recorded with 64 t_1 increments, accumulating 960 scans in each indirect slice with relaxation delay of 4 s, resulting in 3 days of experimental time. Frequency discrimination during the evolution period was achieved with STATES-TPPI method [50]. A 45° shifted squared sine bell window function (qsine SSB = 4 in TopSpin) was applied in the indirect dimension, and further zero-filled to 2048 points prior to Fourier transformation. A 90° shifted squared sine bell window function (qsine SSB = 2) was applied in the direct dimension and zero-filled to 1024 data points.

2.8. Pulse sequences

The pulse sequences used in the present work are shown in Fig. 1.

3. Results and discussion

3.1. Standard 1D ^{13}C photo-CIDNP MAS NMR

The standard photo-CIDNP MAS NMR experiment comprises a simple Hahn-echo sequence acquired under continuous illumination for the direct observation of strong nuclear polarization on ^{13}C nuclei. Such a 1D spectrum recorded on 5-ALA *R. sphaeroides WT* consists of series of light-induced emissive (negative) signals between 80 and 170 ppm, which could be assigned to the response from ^{13}C labels of two BChl *a* (P$_L$ and P$_M$) and one BPheo *a* (Φ$_A$), presented in Fig. 2A. The isotope-labeling pattern of photosynthetic cofactors in 5-ALA *R. sphaeroides WT* is presented in Fig. 2B.
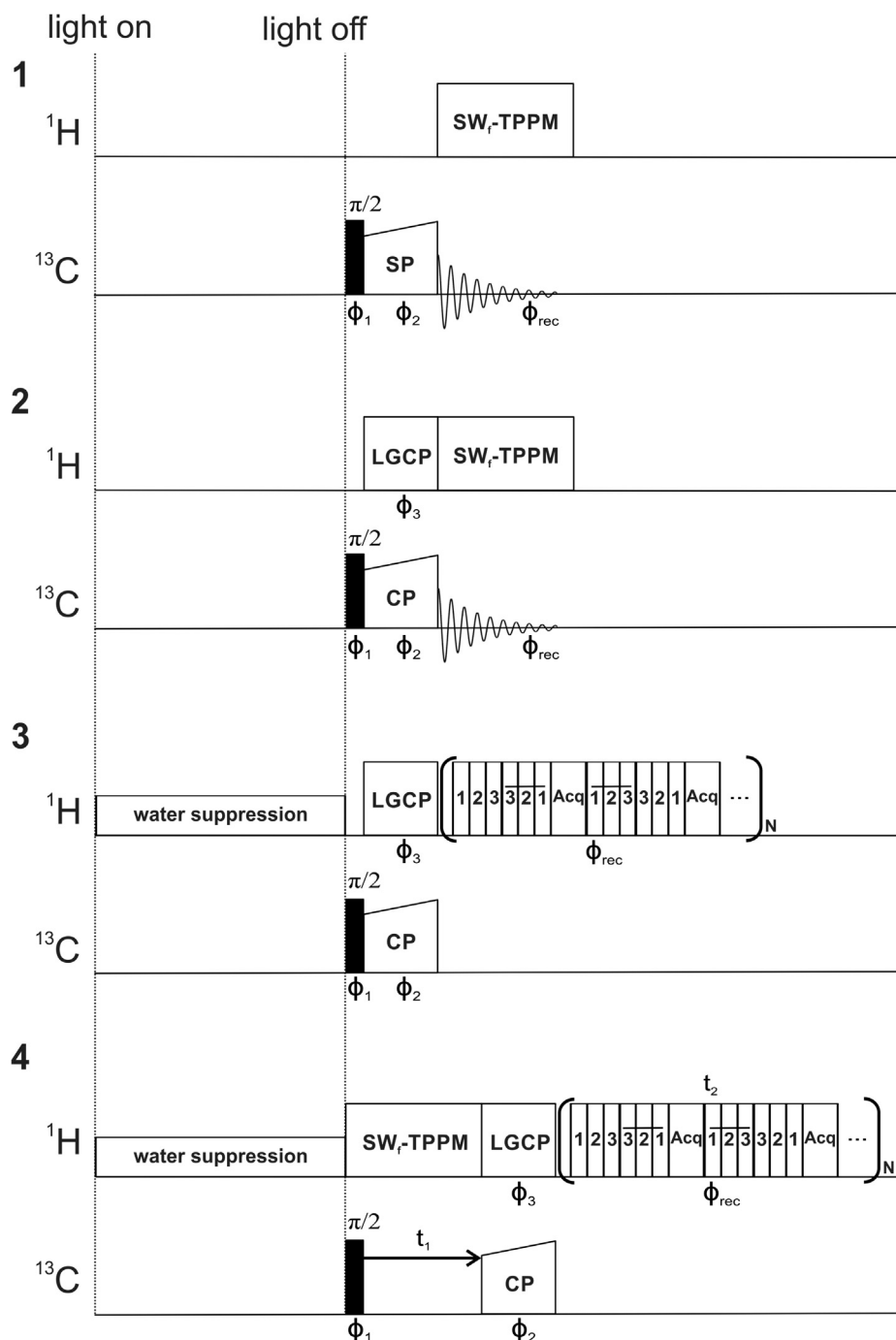
light on   light off

1

^{1}H   SW$_f$-TPPM

$\pi/2$

^{13}C   SP

ϕ_1 ϕ_2 ϕ_{rec}

2

^{1}H   LGCP   SW$_f$-TPPM

ϕ_3

$\pi/2$

^{13}C   CP

ϕ_1 ϕ_2 ϕ_{rec}

3

^{1}H   water suppression   LGCP   1 2 3 3 2 1 Acq 1 2 3 3 2 1 Acq ⋯ N

ϕ_3 ϕ_{rec}

$\pi/2$

^{13}C   CP

ϕ_1 ϕ_2

4

t_2

^{1}H   water suppression   SW$_f$-TPPM   LGCP   1 2 3 3 2 1 Acq 1 2 3 3 2 1 Acq ⋯ N

ϕ_3 ϕ_{rec}

$\pi/2$ t_1

^{13}C   CP

ϕ_1 ϕ_2

Fig. 1. Pulse sequences used to study ^{13}C → ^{1}H polarization transfer. 1D experiment to study the ^{13}C polarization decay due to ^{13}C → ^{1}H transfer consists of the 90° excitation pulse on carbon followed by the spin-lock (SP) pulse on ^{13}C channel (1) or on both channels to satisfy HH condition (2) and ^{13}C acquisition with high power decoupling; ϕ_1 = +y − y − y + y; ϕ_2 = +x; ϕ_3 = +x; ϕ_{rec} = +y − y − y + y. 1D experiment to study the ^{1}H polarization build-up due to ^{13}C → ^{1}H transfer consists of the water suppression block, 90° excitation pulse on carbon followed by the spin-lock pulses on both channels to satisfy HH condition and ^{1}H windowed acquisition with wPMLG3-S2; ϕ_1 = +y − y; ϕ_2 = +x; ϕ_3 = +x + x − x − x + y + y − y − y; ϕ_{rec} = +x − x − x + x + y − y − y + y (3). 2D ^{13}C → ^{1}H correlation experiment consists of the water suppression block, 90° excitation pulse on carbon, the evolution period t_1 during which high power heteronuclear decoupling is applied, two spin-lock pulses to satisfy HH condition and ^{1}H windowed acquisition with wPMLG3-S2; ϕ_1 = +y -y; ϕ_2 = +x; ϕ_3 = +x + x − x − x + y + y − y − y; ϕ_{rec} = +x − x − x + x + y − y − y + y (4). Defined illumination period of 4 s was provided with mechanical shutter triggered via pulse program.

The emissive character of the light-induced signals has been explained previously by the dominance of the three-spin mechanism (TSM) over the differential decay (DD) in the absence of the differential relaxation (DR) mechanism [18,51]. Direct excitation of ^{13}C nuclei does not impose special limit on the repetition delay due to slow relaxation nor does it require special modification of a sample such as paramagnetic doping in order to decrease the longitudinal relaxation time [52]. Since the recovery of the solid-state photo-CIDNP generated signal is faster than the T_1 limit [53], a recycle delay of 4 s, typical for classical ^{1}H–^{13}C CP experiments, is sufficient for photo-CIDNP MAS NMR experiments. With in this time ~50% of steady-state photo-CIDNP signal is reached.
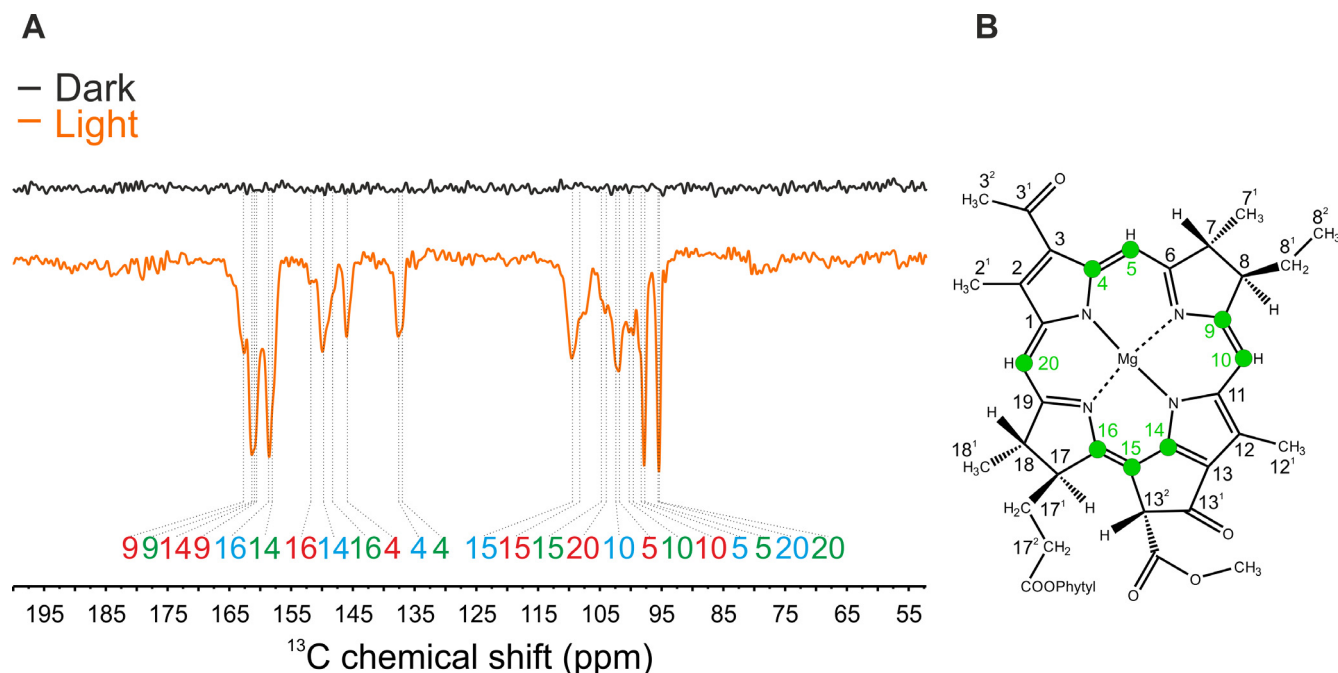
Fig. 2. (A) ^{13}C photo-CIDNP MAS NMR spectra of 5-ALA *R. sphaeroides WT* recorded with Hahn-echo pulse sequence at 9.4 T and MAS frequency of 8176 Hz at 247 K in dark (top) and under continuous illumination (bottom). The colour code of the numbers refers to the assignment to the three cofactors forming the spin correlated radical pair: green, red and blue refer to the two BChl *a* molecules of the donor (P$_L$ and P$_M$) and the acceptor (Φ$_B$), respectively. The assignment of the individual signals is based on the previous work [24]. (B) Isotope labeling pattern of BChl *a* obtained by feeding bacteria with δ-aminolevulinic acid ^{13}C labeled at position 5 (5-ALA). Green circles indicate the positions of ^{13}C labels. The numbering of carbon atoms is according to IUPAC. The molecule of BPheo *a* has an identical labeling pattern.

3.2. ^{13}C → ^{1}H hyperpolarization transfer and carbon acquisition

To study the possibility of transferring the enhanced polarization from ^{13}C to ^{1}H, we performed a series of spin-lock experiments using the pulse sequences presented in Fig. 1(**1–4**). Such pulse sequences are based on inverse polarization transfer, which is unusual in classical applications mainly due to unfavorable carbon polarization in the thermal case, long relaxation times and difficulties in direct proton detection, and therefore used only in specific applications. The few reported cases of utilizing the inverse CP include, for example, the assignment of the proton signals in solid inorganic compounds [54], the study of the dynamics of the fullerene-70 solvated in toluene [55], the study of ion adsorption on microporous materials [56] and the assignment of aliphatic protons in randomly protonated proteins by using CCH sequence [57]. Photo-CIDNP, on the other hand, creates a state in which ^{13}C nuclei are hyperpolarized, *i.e.* they have much lower spin temperature compared to ^{1}H nuclei, therefore the efficient flow of polarization from carbon to proton during CP is expected upon spin locking, leading to the boost of the polarization of protons. This polarization exchange is governed only by the strength of the heteronuclear dipolar couplings between ^{13}C and ^{1}H and the respective rates of the relaxation in the rotating frame (T$_{1\rho}$), mainly T$_{1\rho}^H$. The locking of protons under LG condition provides longer T$_{1\rho}^H$ relaxation time due to the reduced strength of ^{1}H–^{1}H homonuclear dipolar couplings. This assures more selective transfer between ^{13}C–^{1}H pairs [58], therefore simplifying the assignment of heteronuclear correlation experiments and allowing for accurate measurements of ^{1}H–^{13}C distances [59].

The possible ^{13}C → ^{1}H transfer of hyperpolarization can be studied either by detecting the residual ^{13}C polarization after CP transfer similar to CP-drain experiments [60] or by detecting the build-up of ^{1}H polarization directly. In the first set of experiments, we used sequences **1** and **2** and expected to observe the decay of ^{13}C hyperpolarization presumably due to ^{13}C → ^{1}H polarization trans-

fer upon spin locking. The pulse sequence **1** serves as a reference, it starts with illumination period of 4 s during which hyperpolarization builds up on ^{13}C nuclei of special pair and Φ$_A$ due to the solid-state photo-CIDNP effect. The 90^0-^{13}C excitation pulse creates transverse ^{13}C magnetization which is locked with subsequent spin-lock pulse before detection.

The resultant spectra recorded on 5-ALA *R. sphaeroides WT* with three different contact times are presented in Fig. 3 (A–C). They resemble the pattern obtained with Hahn-echo experiment with slight decrease in the signal intensity due to the spin–lattice relaxation of the carbon magnetization in the rotating frame T$_{1\rho}^C$, which is more pronounced upon application of a long contact time. In the second series acquired with pulse sequence **2**, the spin-lock pulse was applied on both ^{13}C and ^{1}H channels with the power to satisfy HH conditions. The results are presented in Fig. 3 (A′–C′).

Already after 80 μs of locking time (Fig. 3A′), the significant drop of the signal intensity of about 60% was observed in the region belonging to the response from carbons 5, 10 and 20 (∼100 ppm), the only ones that have directly attached protons, while the signals originating from the quaternary carbons are not influenced by ^{1}H spin lock. This observation is consistent with direct LGCP experiments under MAS, where the carbon signal intensity shows an oscillatory behavior as a function of contact time, with maximum signal intensity usually obtained under 100 μs contact time for CH moiety, depending on the strength of the heteronuclear dipolar coupling [60]. Since CP is a coherent process, similar behavior happens for ^{13}C → ^{1}H transfer. Therefore, this loss of ^{13}C signal intensity might imply the polarization transfer from carbons C-5, C-10 and C-20 to directly attached protons. Upon increasing the contact time to 500 μs (Fig. 3B′), the slight drop in intensity was also observed for the signals originating from quaternary carbons in region between 104 and 170 ppm, implying their contribution to polarization transfer. Finally, only 20% of the original intensity is left after a long contact pulse of 4500 μs
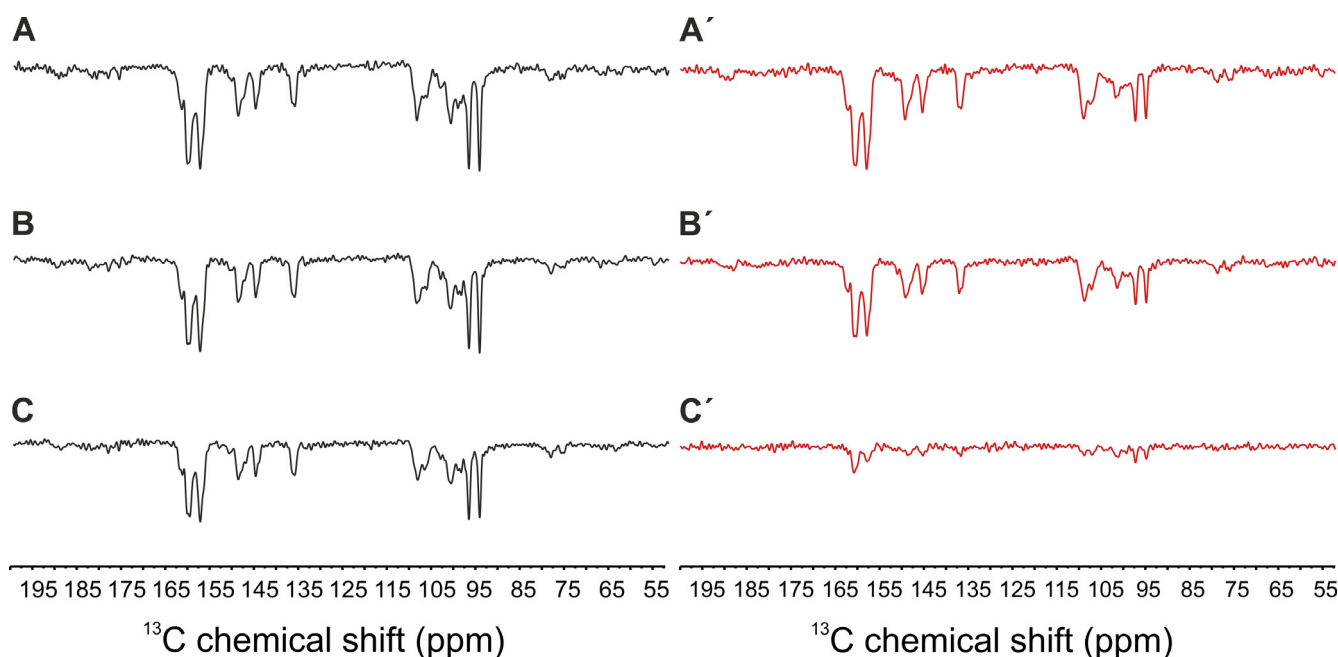
Fig. 3. ^{13}C photo-CIDNP MAS NMR spectra of 5-ALA *R. sphaeroides WT* recorded using pulse sequences 1 and 2 at 9.4 T and MAS frequency of 8176 Hz at 247 K under continuous illumination. No RF power was applied on ^{1}H lock pulse with duration of (A) 80 μs, (B) 500 μs and (C) 4500 μs. Appropriate RF power to satisfy HH condition was applied on ^{1}H lock pulse with duration of (A′) 80 μs, (B′) 500 μs and (C′) 4500 μs.

(Fig. 3C′), which suggests almost complete transfer of ^{13}C polarization into the proton pool.

3.3. $^{13}C \rightarrow {}^1H$ hyperpolarization transfer and proton acquisition

In order to verify that the magnetization is transferred to the protons, we aimed to detect the build-up of the ^{1}H polarization caused by the ^{13}C → ^{1}H transfer. Direct proton detection in frozen non-deuterated membrane protein is challenging due to the network of strongly coupled protons, since the ^{1}H–^{1}H dipolar interactions need to be averaged out at ultrafast MAS frequencies. Alternatively, windowed acquisition with homonuclear decoupling at slow and moderate MAS frequencies has proven to be very effective in resolving ^{1}H spectra of proteins, often being comparable to the performance of fast MAS beyond 60 kHz [61]. Frequently, direct proton detection results in crowded spectra due to the strong signals originating from the solvent and buffer added to the MAS rotor. These undesirable signals usually have much stronger intensities than the signals of interest, and could also overlap with the spectral region of interest. Therefore, the solvent saturation block is often included into the pulse sequences aimed at direct proton detection, which allows to completely eliminate or to reduce the unwanted signals [62]. The pulse sequence **3** proposed for observation of the build-up of ^{1}H hyperpolarization due to ^{13}C → ^{1}H polarization transfer was constructed in the following way. It starts with the illumination period of 4 s during which ^{13}C hyperpolarization builds up due to the solid-state photo-CIDNP effect. This period ends with a solvent suppression block on the ^{1}H channel, followed by a short delay period of 0.1 s that ensures complete closure of a shutter window. A subsequent 90^0 ^{13}C excitation pulse is followed by the application of ramped amplitude spin-lock pulse on the ^{13}C channel together with ^{1}H spin-lock pulse at the LG offset. Finally, direct proton acquisition is achieved with wPMLG3-S2. Implementation of the supercycle into the homonuclear decoupling generates an effective z-rotation for the transverse magnetization, resulting in the suppression of the strong carrier peak and more robust scaling factor over

a wide range of the resonance offsets. Since LGCP generates an off-resonance ^{1}H field that is applied in the way that in the rotating frame the effective field is inclined at the magic angle with respect to the static field in the z-direction, the magnetization generated at ^{1}H channel is expected to be inclined in the similar way parallel to the effective field. In principle, the ^{1}H magic-angle pulse of 35° can be introduced after LGCP to tilt the generated magnetization into the xy-plane with intend to increase the detected signal intensity. However, from our experience, the introduction of such magic-angle pulse neither provides any gain of intensity nor improves the resolution (data not shown).

Fig. 4 shows the ^{13}C photo-CIDNP enhanced 1D ^{1}H MAS NMR spectra from 5-ALA *R. sphaeroides WT* obtained with pulse sequence **3** using three different contact times. No signal was detected in the absence of illumination regardless of the LGCP contact time (Fig. 4A–C). We found that the exact proton transmitter frequency was not critical for solvent suppression. Placing the offset on the strongest peak corresponding to water signal effectively suppressed additional solvent response originating from the detergent and buffer. Upon illumination, the 80 μs contact generates strong signal that occurs at about 8 ppm (Fig. 4A′). Interestingly, the signal has an emissive character, which demonstrates the conservation of the sign of transferred polarization. Longer contact times lead to the growing signals in the aliphatic region of the spectrum (Fig. 4B′ and C′). These results are consistent with the drop of the carbon signal intensity in the ^{13}C-detected experiments. At short contact times, polarization transfer occurs only between close ^{13}C–^{1}H pairs, therefore the signal at ∼8 ppm must originate from protons directly attached to carbons C-5, C-10 and C-20. Such chemical shifts are expected for the protons of the methine bridges of BChl *a* and BPheo *a* [63]. To confirm the emissive character of the ^{1}H signals from 5-ALA *R. sphaeroides WT*, the sequence **3** was repeated on U-^{13}C L-alanine. This sample has fast ^{13}C spin lattice relaxation allowing for short recycle delay in the experiments with direct carbon excitation. The spectra acquired with different contact times resulted in ^{1}H proton spectra with absorptive line shapes similar to pulse-acquire experiment with
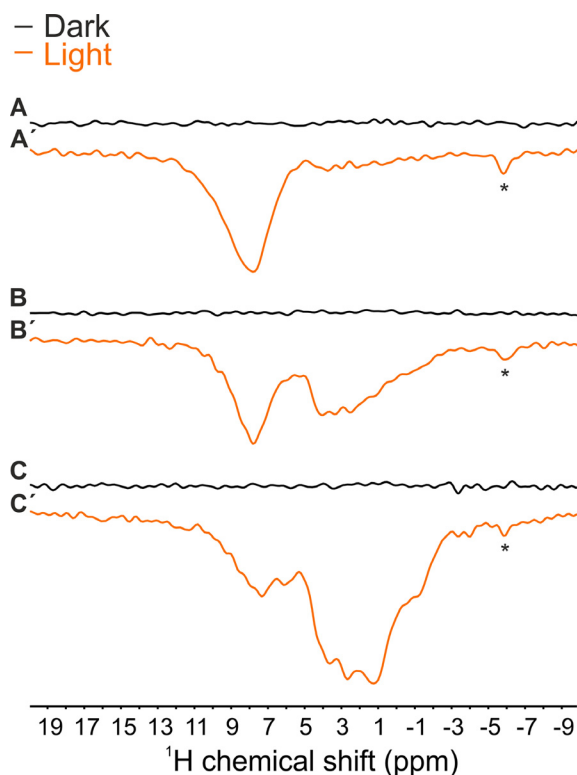
Fig. 4. The photo-CIDNP enhanced 1D ^{1}H MAS NMR spectra from 5-ALA *R. sphaeroides WT* obtained with pulse sequence 3 at 9.4 T and MAS frequency of 8176 Hz in the dark with LGCP contact time of (A) 80 μs, (B) 500 μs and (C) 4500 μs, and upon continuous illumination with LGCP contact time of (A′) 80 μs, (B′) 500 μs and (C′) 4500 μs. The signal labeled with an asterisk refers to an artifact rising from homonuclear decoupling. The spectra were phased according to U-^{13}C labeled L-alanine.

3.4. Photo-CIDNP ^{13}C → ^{1}H HETCOR MAS NMR experiment with proton acquisition

The pulse sequence **4** is proposed for 2D photo-CIDNP ^{13}C → ^{1}H HETCOR MAS NMR experiment. It resembles the sequence **3** with addition of the evolution period t_1 during which the high-power heteronuclear dipolar decoupling is applied on ^{1}H channel. During the maximum t_1 delay time of 2.5 ms, the solvent signals recovered not more than 5% of the intensity. In case when fast spinning is used, the saturation block can be placed directly before the CP part for the best solvent suppression performance. However, in such an implementation at 8 kHz MAS frequency, ^{13}C–^{13}C residual homonuclear dipolar couplings will cause a fast diffusion among ^{13}C spins during z-storing, resulting in the diminishing of the selectivity of the correlation experiment. Therefore, solvent suppression was placed before t_1 evolution similar to Zhou et al. [65]. This implementation also eliminates the potential loss of the signal intensity due to ^{13}C T_1 relaxation while storing magnetization on ^{13}C sites. The correct performance of the pulse sequence **4** was confirmed on a test sample of U-^{13}C L-alanine (Fig. SI 3).

The spectrum in Fig. 5 A recorded at a short contact time on 5-ALA *R. sphaeroides WT* contains one correlation peak located at ~8 ppm in ^{1}H dimension and ~100 ppm in ^{13}C dimension. This proves
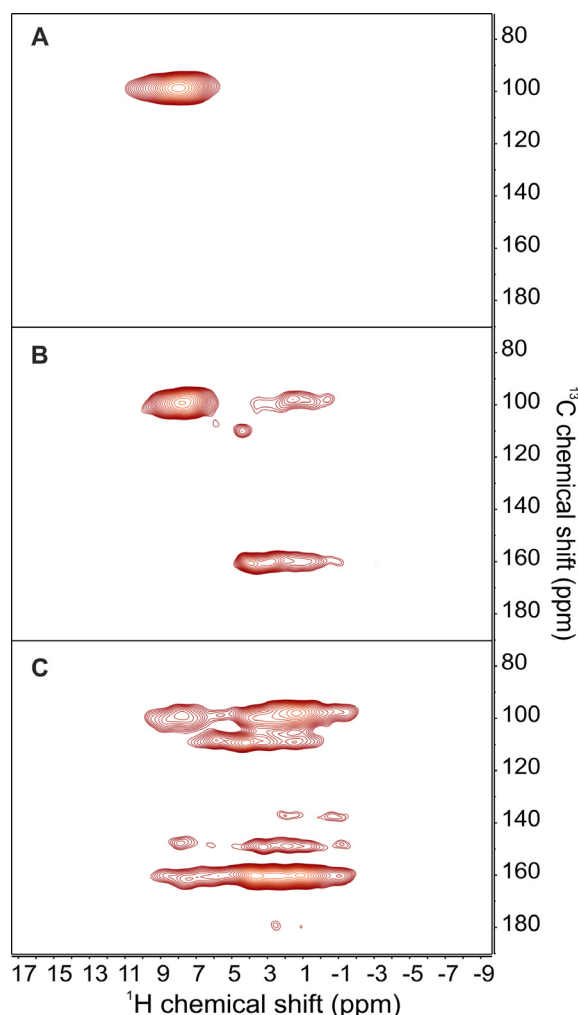
windowed acquisition. Since the sign of the transferred polarization is maintained, we predict that the spectral-editing experiments with laser-flash setup [64], in which the absorptive-emissive patterns of the ^{13}C spectra are observed, will be feasible also for heteronuclear photo-CIDNP MAS NMR experiments. This might allow for sorting the ^{1}H signals based on the sign of the signal from neighboring ^{13}C nucleus, which would simplify the assignment of the proton spectra.

Upon increasing the contact time more, long-distance transfers occur from carbons C-14, C-15, C-16, C-9 and C-4 to nearby protons, presumably H-17, H-18, H-13^2, H-8, and H-7, which are expected in the range of chemical shifts between 6 and 1 ppm. Finally, at a very long contact time the intensity of the signals in a very shielded region increases which might correspond to the transfers to peripheral protons, H-2^1, H-7^1, H-8^1, H-12^1 and H-18^1. Meanwhile, the intensity of the peak around 8 ppm decreases gradually with increasing contact time, which might be attributed to the $T_{1\rho}^H$ relaxation, that happens on a faster timescale as compared with carbons. Therefore, the experiments with both ^{13}C and ^{1}H acquisition proved the feasibility of inverse cross polarization as a means to transfer photo-induced hyperpolarization from carbons to nearby protons. Light-induced signals can be detected already after 10 min of measurement time, and the experimental time of 2 h guarantees good signal-to-noise ratio. However, even with the use of homonuclear decoupling the quality of the ^{1}H spectrum does not allow for the assignment of the individual proton responses due to the broad lines. To overcome this problem, we introduced the second dimension in which proton resonances are resolved according to the chemical shifts of neighboring carbon nuclei.

Fig. 5. Photo-CIDNP ^{13}C–^{1}H HETCOR MAS NMR spectra of 5-ALA *R. sphaeroides WT* recorded with pulse sequence 4 at 9.4 T, temperature of 247 K and a MAS frequency of 8176 Hz under continuous illumination with LGCP contact time of (A) 80 μs, (B) 500 μs and (C) 4500 μs.

the previous assumption that this ^{1}H signal indeed corresponds to a transfer from carbons C-5, C-10 and C-20 as they all appear between 103 and 95 ppm. 64 points in the indirect domain were not enough to distinguish the individual signals from P_L, P_M and Φ_A, as they all fall into narrow range of chemical shifts. The 500 µs and 4500 µs LGCP contacts provide many more correlation peaks. Based on an approximate cut-off distance of about 3 Å and <4 Å for 500 µs and 4500 µs, respectively, as was estimated by recording classical ^{1}H–^{13}C LGCP HETCOR on L-tyrosine hydrochloride and comparing the correlation peaks with the intra-inter molecular distances taken from neutron diffraction data [59,66], it was possible to perform a tentative assignment of some of the correlation peaks (Fig. SI 4). A cut-off at 4 Å already enables the possibility for intermolecular correlations between the bacteriochlorophylls of the special pair and also with nearby amino acids, which complicates the assignment. Signal at $\delta^H \sim 8$ ppm also has multiple correlations around 160 ppm in ^{13}C dimension, which might be due to contacts between protons H-10 and H-20 and carbons C-9 (P_L, P_M, Φ), C-14 (P_L, P_M) and C-16 (Φ), that have similar chemical shifts between 162.1 and 157.5 ppm. The last correlation at $\sigma^H \sim 8$ ppm and ^{13}C at $\sim$148 ppm could be H-20/C-16 (P_L, P_M) and H-5/C-4 (P_M). Surprisingly, correlations H-5/C-4 and H-10/C-9 located only 2.1 Å apart are not visible at 500 µs contact time. The signal at $\delta^H \sim 5.9$ ppm correlates with C-15 (104.2–108.8 ppm), and at 4500 µs also to C-16 and C-14 (160.1–157.5 ppm), we therefore assign it to H-13^2. The signal at $\delta^H \sim 4.4$ ppm has high intensity already at 500 µs and correlates with C-15 and C-16 (Φ). It is therefore assigned to H-17. At 500 µs signal at $\delta^H \sim 3.7$ ppm has a strong correlation with carbons C-9 (162–157 ppm) and a weaker correlation with C-10 (at $\sim$100 ppm). The latter correlation is more pronounced at longer contact. For this reason, we tentatively assign the resonance at 3.7 ppm to proton H-8. Signals between $\delta^H \sim 2.5$ and 1.1 ppm have strong correlations with C-9 and C-16 and weaker with C-5, C-10 and C-20, since probably they belong to protons H-8^1 and H-17^1. Signals in the very shielded region from 1 ppm to −1.5 ppm show up only at very long contact time and should belong to peripheral protons H-8^2, H-2^1, H-3^2. The relative positions of the three groups of proton signals seem to follow the general tendency observed for isolated BChl a, with increasing shielding effect starting from the methine bridges up to aromatic and peripheric protons. The relative positions of the individual proton signals must be further investigated. Thus, in order to rationalize the effect of protein environment on the chemical shifts of protons, the ring current effects must be taken into account [67], as the two almost identical porphyrin molecules of the special pair are located in the close to each other (with only $\sim$3.4 Å intermolecular distance between P_L and P_M).

Overall, the photo-CIDNP HETCOR MAS NMR experiment with ^{13}C → ^{1}H hyperpolarization transfer provided strong correlation signals in a relatively short amount of time. The resultant ^{1}H signals are selective and originate from the labeled cofactors and probably their close protein environment, while the rest of the backbone signals are not observed. The signal build-up was detected even after 64 t_1 points, which allows in principle to increase the resolution in F_1 dimension by accumulating more indirect increments. The resolution in ^{1}H dimension could be further improved by combining simultaneous homonuclear and heteronuclear decoupling [68]. Meanwhile, the classical LGCP HETCOR with ^{1}H → ^{13}C transfer performed in our setup at 9.4 T magnetic field and 8 kHz MAS frequency and 7 days of the measurement time failed to show the correlation signals on the selective cofactors, resulting only in the crowded upfield region belonging to the protein backbone, both in dark and under illumination (data not shown). Experiments at higher field and MAS frequency might reveal as well the signals from the cofactors. However, since the isotopic labeling procedure with the use of

δ-aminolevulinic acid results in the RCs in which *all* bacteriochlorophylls and bactriopheophytins are labeled, we predict the higher complexity of the classical ^{1}H → ^{13}C correlation spectra which would consists of the feedback from 6 almost identical cofactors including the ones that are highlighted by photo-CIDNP plus the accessory BChls a (B_A and B_B) and BPheo a (Φ_B) and the backbone signals, which would overlap with the signals from the side chains of the special pair.

To be able to detect the polarization transfers from the ^{13}C nuclei of the cofactors to the close protein environment in ^{13}C → ^{1}H experiment, the map of the chemical shifts of protons belonging to the special pair and Φ_A will be required. To that end, different ^{13}C-labelling patterns can be probed with short LGCP contact times to assure only 1-bond correlations. In the previous works 2-ALA, 3-ALA and 4-ALA selectively labeled reaction centers have been successfully produced [69], covering almost the whole range of aromatic and aliphatic carbons. These RCs will be tested with the proposed photo-CIDNP ^{13}C → ^{1}H HETCOR MAS NMR experiment.

4. Conclusions

In the present study, we have performed ^{13}C → ^{1}H heteronuclear transfer of photo-CIDNP-generated hyperpolarization occurring in the frozen photosynthetic protein complex. With the sample illumination and moderate cooling as the only setup requirements, these types of experiments are easy to perform, as was demonstrated on the selectively ^{13}C reaction center from *R. sphaeroides WT*. The first proton chemical shifts of the electron donor and acceptor in their native environment have been obtained, suggesting the behavior of the general trends of the chemical shifts between the special pair and isolated bacteriochlorophyll. We expect that the proposed approach has a potential for a heteronuclear photo-CIDNP spin-torch to explore the protein vicinity around the special pair, thus broadening the potential application of photo-CIDNP MAS NMR technique. The feasibility of the inverse cross polarization as means to hyperpolarization transfer suggests the possibility to implement solid-state photo-CIDNP enhancement step in almost any CP-based NMR pulse sequence, for example MELODI-HETCOR [70], thus providing more tools for studying the protonic state of donor-acceptor pairs and their close environment in the photosynthetic reaction centers, including photosystem II of plants.

Appendix A. Supplementary material

Supplementary data associated with this article can be found, in the online version, at https://doi.org/10.1016/j.jmr.2018.06.003.

References

[1] V. Ladizhansky, Applications of solid-state NMR to membrane proteins, BBA Proteins Proteom. 1865 (2017) 1577–1586.
[2] L.T. Kuhn (Ed.), Hyperpolarization Methods in NMR Spectroscopy, Springer, 2013, pp. 1–304.
[3] A. Bornet, R. Melzi, A.J.P. Linde, P. Hautle, B. van den Brandt, S. Jannin, G. Bodenhausen, Boosting dissolution dynamic nuclear polarization by cross polarization, J. Phys. Chem. Lett. 4 (2013) 111–114.

[4] M. Batel, A. Däpp, A. Hunkeler, B. Meier, S. Kozerke, M. Ernst, Cross-polarization for dissolution dynamic nuclear polarization, Phys. Chem. Chem. Phys. 16 (2014) 21407–21416.

[5] J. Milani, B. Vuichoud, A. Bornet, R. Melzi, S. Jannin, G. Bodenhausen, Hyperpolarization of nitrogen-15 nuclei by cross polarization and dissolution dynamic nuclear polarization, Rev. Sci. Instrum. 88 (2017), 015109-1–015109-5.

[6] H.C. Gaede, Y.-Q. Song, R.E. Taylor, E.J. Munson, J.A. Reimer, A. Pines, High-field cross polarization NMR from laser-polarized xenon to surface nuclei, Appl. Magn. Reson. 8 (1995) 373–384.

[7] K.D. Atkinson, M.J. Cowley, S.B. Duckett, P.I.P. Elliott, G.G.R. Green, J. López-Serrano, I.G. Khazal, A.C. Whitwood, Para-hydrogen induced polarization without incorporation of para-hydrogen into the analyte, Inorg. Chem. 48 (2009) 663–670.

[8] S. Knecht, A.S. Kiryutin, A.V. Yurkovskaya, K.L. Ivanov, Re-polarization of nuclear spins using selective SABRE-INEPT, J. Magn. Reson. 287 (2018) 10–14.

[9] C.E. Lyon, J.A. Jones, C. Redfield, C.M. Dobson, P.J. Hore, Two-dimensional ^{15}N–^{1}H photo-CIDNP as a surface probe of native and partially structured proteins, J. Am. Chem. Soc. 121 (1999).

[10] M.J. Zysmilich, A. McDermott, Photochemically induced dynamic nuclear polarization in the solid-state 15N spectra of reaction centers from photosynthetic bacteria Rhodobacter sphaeroides R-26, J. Am. Chem. Soc. 116 (1994) 8362–8363.

[11] B.E. Bode, S.S. Tamarath, K.B. Sai Sankar Gupta, A. Alia, G. Jeschke, J. Matysik, The solid-state photo-CIDNP effect and its analytical application, Springer, 2013, pp. 105–121.

[12] J. Matysik, A. Diller, E. Roy, A. Alia, The solid-state photo-CIDNP effect, Photosynth. Res. 102 (2009) 427–435.

[13] J.C. Zill, M. Kansy, R. Goss, L. Köhler, A. Alia, C. Wilhelm, J. Matysik, Photo-CIDNP in the reaction center of the diatom Cyclotella meneghiniana observed by ^{13}C MAS NMR, Z. Phys. Chem. 231 (2017) 347–367.

[14] S.S. Thamarath, J. Heberle, P. Hore, T. Kottke, J. Matysik, Solid-state photo-CIDNP effect observed in phototropin LOV1-C57S by ^{13}C magic-angle spinning NMR spectroscopy, J. Am. Chem. Soc. 132 (2010) 15542–15543.

[15] G. Jeschke, J. Matysik, A reassessment of the origin of photochemically induced dynamic nuclear polarization effects in solids, Chem. Phys. 294 (2003) 239–255.

[16] E. Daviso, G. Jeschke, J. Matysik, Photochemically induced dynamic nuclear polarization (Photo-CIDNP) magic-angle spinning NMR, Springer, Netherlands, 2008, pp. 385–399.

[17] D. Sosnovsky, G. Jeschke, J. Matysik, H.-M. Vieth, K.L. Ivanov, Level crossing analysis of chemically induced dynamic nuclear polarization: towards a common description of liquid-state and solid-state cases, J. Phys. Chem. 144 (2016) 144202–144217.

[18] S. Prakash, Alia, Gast, P., de Groot, H. J. M., Matysik, J., Jeschke, G. Photo-CIDNP MAS NMR in intact cells of Rhodobacter sphaeroides R26: molecular and atomic resolution at nanomolar concentration, J. Am. Chem. Soc. 128 (2006) 12794–12799.

[19] G.J. Janssen, E. Daviso, M. van Son, H.J.M. de Groot, A. Alia, J. Matysik, Observation of the solid-state photo-CIDNP effect in entire cells of cyanobacteria Synechocystis, Photosynth. Res. 104 (2010) 275–282.

[20] E. Daviso, G.J. Janssen, A. Alia, G. Jeschke, J. Matysik, M. Tessari, 10000-fold nuclear hyperpolarization of a membrane protein in the liquid phase via a solid-state mechanism, J. Am. Chem. Soc. 133 (2011) 16754–16757.

[21] A.J. Hoff, J. Deisenhofer, Photophysics of photosynthesis. Structure and spectroscopy of reaction centers of purple bacteria, Phys. Rep. 287 (1997) 1–247.

[22] E.A.M. Schulten, J. Matysik, S. Kiihne, J. Raap, J. Lugtenburg, P. Gast, A.J. Hoff, H.J.M. de Groot, ^{13}C MAS NMR and photo-CIDNP reveal a pronounced asymmetry in the electronic ground state of the special pair of Rhodobacter sphaeroides reaction centers, Biochemistry 41 (2002) 8708–8717.

[23] K.B. Sai Sankar Gupta, A. Alia, H.J.M. de Groot, J. Matysik, Symmetry break of special pair: photochemically induced dynamic nuclear polarization NMR confirms control by nonaromatic substituents, J. Am. Chem. Soc. 135 (2013) 10382–10387.

[24] M. Najdanova, D. Gräsing, A. Alia, J. Matysik, Analysis of the electronic structure of the special pair of bacterial photosynthetic reaction center by ^{13}C photochemically induced dynamic nuclear polarization magic-angle spinning NMR using a double-quantum axis, Photochem. Photobiol. 94 (2018) 69–80.

[25] S.S. Tamarath, B.E. Bode, S. Prakash, K.B. Sai Sankar Gupta, A. Alia, G. Jeschke, J. Matysik, Electron spin density distribution in the special pair triplet of Rhodobacter sphaeroides R26 revealed by magnetic field dependence of the solid-state photo-CIDNP effect, J. Am. Chem. Soc. 134 (2012) 5921–5930.

[26] S. Paul, B. Bode, J. Matysik, A. Alia, Photochemically induced dynamic nuclear polarization observed by solid-state NMR in uniformly 13C-isotope labeled photosynthetic reaction center, J. Phys. Chem. B 119 (2015) 13897–13903.

[27] D. Gräsing, P. Bielytskyi, I.F. Céspedes-Camacho, A. Alia, T. Marquardsen, F. Engelke, J. Matysik, Field-cycling NMR with high-resolution detection under magic-angle spinning: determination of field-window for nuclear polarization in a photosynthetic center, Sci. Rep. 7 (12111) (2017) 1–6.

[28] G. Jeschke, B.C. Anger, B. Bode, J. Matysik, Theory of solid-state photo-CIDNP in the Earth's magnetic field, J. Phys. Chem. A 115 (2011) 9919–9928.

[29] J. Rautter, F. Lendzian, C. Schulz, A. Fetsch, M. Kuhn, X. Lin, J.C. Williams, J.P. Allen, W. Lubitz, ENDOR studies of the primary donor cation radical in mutant reaction centers of Rhodobacter sphaeroides with altered hydrogen-bond interactions, Biochemistry 34 (1995) 8130–8143.

[30] K. Artz, J.C. Williams, J.P. Allen, F. Lendzian, J. Rautter, W. Lubitz, Relationship between the oxidation potential and electron spin density of the primary electron donor in reaction centers from Rhodobacter sphaeroides, Proc. Natl. Acad. USA 94 (1997) 13582–13587.

[31] X. Lin, H.A. Murchison, V. Nagarajan, W.W. Parson, J.P. Allen, J.C. Williams, Specific alteration of the oxidation potential of the electron donor in reaction centers from Rhodobacter sphaeroides, Proc. Natl. Acad. Sci. 91 (1994) 10265–10269.

[32] A. Diller, A. Alia, E. Roy, P. Gast, H.J. van Gorkom, J. Zaanen, H.J.M. de Groot, C. Glaubitz, J. Matysik, Photo-CIDNP solid-state NMR on Photosystems I and II: what makes P680 special?, Photosynth. Res. 84 (2005) 303–308.

[33] C. Schlörb, S. Mensch, C. Richter, H. Schwalbe, Photo-CIDNP reveals differences in compaction of non-native states of lysozyme, J. Am. Chem. Soc. 128 (2006) 1802–1803.

[34] A. Sekhar, S. Cavagnero, EPIC- and CHANCE-HSQC: two ^{15}N-photo-CIDNP-enhanced pulse sequences for the sensitive detection of solvent-exposed tryptophan, J. Magn. Reson. 200 (2009) 207–213.

[35] J.H. Lee, A. Sekhar, S. Cavagnero, ^{1}H-detected ^{13}C photo-CIDNP as a sensitivity enhancement tool in solution NMR, J. Am. Chem. Soc. 133 (2011) 8062–8065.

[36] K.R. Mote, V. Agarwal, P.K. Madhu, Five decades of homonuclear dipolar decoupling in solid-state NMR: status and outlook, Prog. Nucl. Magn. Reson. Spectrosc. 97 (2016) 1–39.

[37] R. Zhang, K.H. Mroue, A. Ramamoorthy, Proton-based ultrafast magic angle spinning solid-state NMR spectroscopy, Acc. Chem. Res. 50 (2017) 1105–1113.

[38] S. Prakash, A. Alia, P. Gast, H.J.M. de Groot, G. Jeschke, J. Matysik, ^{13}C Chemical shift map of the active cofactors in photosynthetic reaction centers of Rhodobacter sphaeroides revealed by photo-CIDNP MAS NMR, Biochemistry 46 (2007) 8953–8960.

[39] S. Schochat, T. Arlt, C. Francke, P. Gast, P.I. Vannoort, S.C.M. Otte, H.P.M. Schelvis, S. Schmidt, E. Vijgenboom, J. Vrieze, W. Zinth, A.J. Hoff, Spectroscopic characterization of reaction centers of the (M)Y210W mutant of the photosynthetic bacterium Rhodobacter sphaeroides, Photosynth. Res. 40 (1994) 55–66.

[40] M.Y. Okamura, R.A. Isaacson, G. Feher, Primary acceptor in bacterial photosynthesis – obligatory role of ubiquinone in photoactive reaction centers of Rhodopseudomonas sphaeroides, Proc. Natl. Acad. Sci. U.S.A. 72 (1975) 3491–3495.

[41] M.R. Fischer, H.J.M. de Groot, J. Raap, C. Winkel, A.J. Hoff, J. Lugtenburg, ^{13}C magic angle spinning NMR-study of the light-induced and temperature-dependent changes in Rhodobacter sphaeroides R-26 reaction centers enriched in 4'-^{13}C tyrosine, Biochemistry 31 (1992) 11038–11049.

[42] S. Paul, R.S. Thakur, M. Goswami, A.C. Sauerwein, S. Mamone, M. Concistrè, H. Förster, M.H. Levitt, P.K. Madhu, Supercycled homonuclear dipolar decoupling sequences in solid-state NMR, J. Magn. Reson. 197 (2009) 14–19.

[43] M. Leskes, P.K. Madhu, Vega, S. A broad-banded z-rotation windowed phase-modulated Lee-Goldburg pulse sequence for ^{1}H spectroscopy in solid-state NMR, Chem. Phys. Lett. 447 (2007) 370–374.

[44] C. Coelho, J. Rocha, P.K. Madhu, L. Marfa, Practical aspects of Lee-Goldburg based CRAMPS techniques for high-resolution ^{1}H NMR spectroscopy in solids: implementation and applications, J. Magn. Reson. 194 (2008) 264–282.

[45] E. Vinogradov, P.K. Madhu, S. Vega, Phase modulated Lee-Goldburg magic angle spinning proton nuclear magnetic resonance experiments in solid state: a bimodal Floquet theoretical treatment, J. Chem. Phys. 115 (2001) 8983–9000.

[46] E. Vinogradov, P.K. Madhu, S. Vega, Proton spectroscopy in solid state nuclear magnetic resonance with windowed phase modulated Lee-Goldburg decoupling sequences, Chem. Phys. Lett. 354 (2002) 193–202.

[47] M. Leskes, P.K. Madhu, S. Vega, Proton line narrowing in solid-state nuclear magnetic resonance: New insights from windowed phase-modulated Lee-Goldburg sequence, J. Chem. Phys. 125 (2006) 124506–124518.

[48] R.S. Thakur, N.D. Kurur, P.K. Madhu, Swept-frequency two-pulse phase modulation for heteronuclear dipolar decoupling in solid-state NMR, Chem. Phys. Lett. 426 (2006) 459–463.

[49] M. Lee, W.I. Goldburg, Nuclear-magnetic-resonance line narrowing by a rotating rf field, Phys. Rev. A 140 (1965) 1261–1271.

[50] D. Marion, M. Ikura, R. Tschudin, A. Bax, Rapid recording of 2D NMR spectra without phase cycling. Application to the study of hydrogen exchange in proteins, J. Magn. Reson. 85 (1989) 393–399.

[51] S. Prakash, A. Alia, P. Gast, H.J.M. de Groot, G. Jeschke, J. Matysik, Magnetic filed dependence of photo-CIDNP MAS NMR of photosynthetic reaction centers of Rhodobacter sphaeroides WT, J. Am. Chem. Soc. 127 (2005) 14290–14298.

[52] N.P. Wickramasinghe, M. Kotecha, M. Samoson, J. Past, Y. Ishii, Sensitivity enhancement in ^{13}C Solid-state NMR of protein microcrystals by use of paramagnetic metal ions for optimizing ^{1}H T_1 relaxation, J. Magn. Reson. 184 (2007) 350–356.

[53] A. Diller, S. Prakash, A. Alia, P. Gast, J. Matysik, G. Jeschke, Signals in solid-state photochemically induced dynamic nuclear polarization recover faster than signals obtained with the longitudinal relaxation time, J. Phys. Chem. B 111 (2007) 10606–10614.

[54] R.C. Crosby, R.L. Reese, J.F. Haw, Cross polarization magic angle spinning proton NMR spectroscopy of solids, J. Am. Chem. Soc. 110 (1988) 8550–8551.

[55] W. Kolodziejski, J. Klinowski, ^{13}C → ^{1}H and ^{1}H → ^{13}C cross polarization NMR in toluene-solvated fullerene-70, Chem. Phys. Lett. 247 (1995) 507–509.

[56] A.C. Forse, J.M. Griffin, H. Wang, N.M. Trease, V. Presser, Y. Gogotsi, P. Simon, C.P. Grey, Nuclear magnetic resonance study of ion adsorption on microporous carbide-derived carbon, Phys. Chem. Chem. Phys. 15 (2013) 7722–7730.

[57] S. Asami, B. Reif, Assignment strategies for aliphatic protons in the solid-state in randomly protonated proteins, J. Biomol. NMR 52 (2012) 31–39.

[58] V. Ladizhansky, S. Vega, Polarization transfer dynamics in Lee-Goldburg cross polarization nuclear magnetic resonance experiments on rotating solids, J. Chem. Phys. 112 (2000) 7158–7168.

[59] B.-J. van Rossum, C.P. de Groot, V. Ladizhansky, S. Vega, H.J.M. de Groot, A method for measuring heteronuclear ^{1}H–^{13}C distances in high speed MAS NMR, J. Am. Chem. Soc. 122 (2000) 3465–3472.

[60] S. Ando, R.K. Harris, A. Reinsberg, Analysis of cross-polarization dynamics between two abundant nuclei, ^{19}F and ^{1}H on spin thermodynamics theory, J. Magn. Reson. 141 (1999) 91–103.

[61] K.R. Mote, P.K. Madhu, Proton-detected solid-state NMR spectroscopy of fully protonated proteins at slow to moderate magic-angle spinning frequencies, J. Magn. Reson. 261 (2015) 149–156.

[62] D.H. Zhou, C.M. Riensta, High-performance solvent suppression for proton-detected solid-state NMR, J. Magn. Reson. 192 (2008) 167–172.

[63] T. Egorova-Zachernyuk, B. van Rossum, C. Erkelens, H. de Groot, Characterization of uniformly ^{13}C, ^{15}N labeled bacteriochlorophyll *a* and bacteriopheophytin *a* in solution and in solid state: complete assignment of the ^{13}C, ^{1}H and ^{15}N chemical shifts, Magn. Reson. Chem. 46 (2008) 1074–1083.

[64] K.B. Sai Sankar Gupta, E. Daviso, G. Jeschke, A. Alia, M. Ernst, J. Matysik, Spectral-editing through laser-flash excitation in two-dimensional photo-CINDP MAS NMR experiments, J. Magn. Reson. 246 (2014) 9–17.

[65] D.H. Zhou, G. Shah, M. Cormos, C. Mullen, D. Sandoz, C.M. Rienstra, Proton-detected solid-state NMR spectroscopy of fully protonated proteins at 40 kHz magic-angle spinning, J. Am. Chem. Soc. 129 (2007) 11791–11801.

[66] N.M. Frey, T.F. Koetzle, M.S. Lehmann, W.C. Hamilton, Precision neutron diffraction structure determination of protein and nucleic acid components. A comparison between the crystal and molecular structures of L-tyrosine and L-tyrosine hydrochloride, J. Chem. Phys. 58 (1973) 2547–2556.

[67] C. Giessner-Prettre, B. Pullman, Intermolecular nuclear shielding due to the aromatic amino acids of proteins and to porphyrins, J. Theor. Biol. 31 (1971) 287–294.

[68] K.R. Mote, P.K. Madhu, Simultaneous homonuclear and heteronuclear spin decoupling in magic-angle spinning solid-state NMR, Solid State Nucl. Magn. Reson. 90 (2018) 7–12.

[69] K.B. Sai Sankar Gupta, A. Alia, F. Buda, H.J.M. de Groot, J. Matysik, Bacteriopheophytin *a* in the active branch of the reaction center of *Rhodobacter sphaeroides* is not disturbed by the protein matrix as shown by ^{13}C photo-CIDNP MAS NMR, J. Phys. Chem. B 117 (2013) 3287–3297.

[70] X.L. Yao, K. Schmidt-Rohr, M. Hong, Medium- and Long-Distance ^{1}H–^{13}C heteronuclear correlation NMR in solids, J. Magn. Reson. 149 (2001) 139–143.